Base Dynamics of Local Z-DNA Conformations As Detected by Electron Paramagnetic Resonance with Spin-Labeled Deoxycytidine Analogues†

Oliver K. Strobel, Robert S. Keyes, and Albert M. Bobst*
Department of Chemistry, University of Cincinnati, Cincinnati, Ohio 45221
Received June 13, 1990; Revised Manuscript Received July 18, 1990

ABSTRACT: Conformational detection and base dynamics of spin-labeled Z-DNA have been investigated by electron paramagnetic resonance (EPR) spectroscopy. The two synthesized and characterized probes used in this study were C(5)-nitroxide-labeled 2′-deoxycytidine 5′-triphosphates, pppDCAT and pppDCAVAT, which serve as suitable substrates for *Micrococcus luteus* DNA polymerase. Enzymatic incorporation of these probes into $(dG\text{-}dC)_n$ yields the EPR-active alternating copolymers $(dG\text{-}dC,DCAT)_n$ and $(dG\text{-}dC,\text{-}DCAVAT)_n$. These polymers assume typical B- and Z-DNA conformations under respective low (0.1 M NaCl) and high (4.5 M NaCl) salt conditions, as evidenced by their UV–circular dichroism spectra. The EPR line shape of $(dG\text{-}dC,DCAT)_n$ in Z-form is unique and significantly different from the B-form EPR spectrum. A similar observation is made for $(dG\text{-}dC,DCAVAT)_n$. Thus, the EPR line shapes of these spin-labeled DNAs are indicative of their local conformations. The EPR spectra, analyzed with a previously published motional model [Kao, S.-C., Polnaszek, C. F., Toppin, C. R., & Bobst, A. M. (1983) *Biochemistry 22*, 5563–5568], indicate $\tau_\perp$ values of 4 and 7 ns for the B- and Z-forms, respectively. Therefore, the base dynamics of Z-DNA are about two times slower than in B-DNA.

Since the discovery of Z-form DNA (Pohl & Jovin, 1972; Wang et al., 1979; Drew et al., 1980) and RNA (Hall et al., 1984), laboratories worldwide have worked to identify and characterize this interesting nucleic acid conformation in an attempt to establish its function in nature. Significant strides have been made in answering the questions and removing the doubts that once surrounded Z-DNAs possible significance or biological existence (Marx, 1985). The body of evidence is continuously growing, which supports the hypothesis that Z-DNA and other non-B-DNA structures, which generate the conformational microheterogeneity in DNA, exist in vivo (Zacharias et al., 1988) and play fundamental roles in genetic regulation.

Several methods of studying Z-DNA employ sensitive chemical or enzymatic probes that can effectively determine the presence of such local structures under physiologically relevant conditions in vitro and also in vivo (Kochel & Sinden, 1989). Recently, it was shown that local Z-DNA conformations were readily detected spectroscopically by EPR[1] in conjunction with nitroxide spin labels (Strobel et al., 1990). Several other nucleic acid conformations, including single strands, double-stranded A- or B-forms (Kao et al., 1985), and hairpin loops (Spaltenstein et al., 1989b), have been similarly identified by their unique EPR signatures. However, this technique is not limited solely to empirical conformation recognition, as are many local Z-DNA assays; instead, dynamics information can also be extracted from EPR spectra, specifically, nanosecond base motions.

Evidence for internal oscillatory motions in DNA was recognized by using fluorescence intercalators bound to the helix (Wahl et al., 1970). NMR has been used to observe internal motions in the B- and Z-conformations of DNA oligomers (Mirau et al., 1985; Ikuta & Wang, 1989). Spin labeling of bases with nitroxides provides a means of observing the nature of these motions. With respect to the diffusion of a nitroxide tethered to a base of DNA, two models have been used to successfully interpret EPR spectra. This laboratory has used an anisotropic model characterized by two correlation times ($\tau_\perp$, $\tau_\parallel$). We found that an isotropic model, characterized by a mean correlation time [$\tau_R = (\tau_\parallel\tau_\perp)^{1/2}$], does not provide good simulation of our data. The base is modeled as a disk (base disk model), which is distinguished from intercalator models that consider the base pair to be the disk. The assembly of the nitroxide tethered to the base is defined as the diffusing system. The principal diffusion axis is considered to coincide with an axis defined by the bond connecting the tether to the base. This model has been successfully applied to over 40 DNA and RNA systems with thymidylates and deoxycytidylates substituted in position 5 with nitroxides that use tethers varying in length from 2 to 11 atoms (Kao et al., 1983; Kao & Bobst, 1985; Pauly et al., 1987; Strobel et al., 1989). A key element of this model is that base motion contributes significantly to the dynamics of the system. Base dynamics may include tilting, twisting, and torsional components that collectively are represented by $\tau_\perp$. We have consistently observed a $\tau_\perp$ of 4 ns in double-stranded systems and have also observed that this value is independent of the helix length with the five-atom-tethered DUAT (Bobst et al., 1988). The faster of the correlation times, $\tau_\parallel$, is tether dependent, less

† This work was supported in part by NIH Grant GM-27002.
* Author to whom correspondence should be addressed.

[1] Abbreviations: EPR, electron paramagnetic resonance; HPLC, high-performance liquid chromatography; FPLC, fast protein liquid chromatography; NMR, nuclear magnetic resonance; UV, ultraviolet; CD, circular dichroism; TMAC, tetramethylammonium chloride; TLC, thin-layer chromatography; pppDCAT, 5-[3-(2,2,6,6-tetramethyl-1-oxypiperidine-4-carboxamido)prop-1-enyl]-2′-deoxycytidine 5′-triphosphate (**5**); pppDCAVAT, 5-{3-[5-(2,2,6,6-tetramethyl-1-oxypiperidine-4-carboxamido)pentanamido]prop-1-enyl}-2′-deoxycytidine 5′-triphosphate (**6**); $(dI\text{-}dC)_n$, alternating copolymer of deoxyinosine and deoxycytidine; $(dG\text{-}dC)_n$, alternating copolymer of deoxyguanosine and deoxycytidine; $(dG\text{-}dC,dL)_n$, randomly spin-labeled alternating copolymer of deoxyguanosine and deoxycytidine where some of the dC residues are substituted by the spin-labeled deoxycytidine analogue; dL, any spin-labeled deoxycytidine analogue (either DCAT or DCAVAT); DTT, dithiothreitol; POPOP, 1,4-bis(5-phenyl-2-oxazolyl)benzene; PPO, 2,5-diphenyloxazole; $\tau_\parallel$, correlation time describing diffusion about the principal axis; $\tau_\perp$, correlation time describing diffusion perpendicular to the principal axis; h_+, height of low-field line; h_0, height of center-field line; h_-, height of high-field line.

0006-2960/90/0429-8522$02.50/0

than 1 ns, and is attributed to nitroxide motion independent of base motion. We have found that $\tau_{\parallel}$ decreases as the tether length increases, suggesting that longer tethers are less rigid than short tethers.

Spaltenstein et al. (1989a) used an isotropic model to analyze their EPR spectra, where the DNA helix is considered to be the diffusing system. This model was successfully applied to analyze spin-labeled systems containing thymidylate substituted in position 5 with a nitroxide employing a two-atom acetylene tether. Correlation times obtained from simulation of EPR data were compared to values calculated by hydrodynamic theory for the diffusion of a rigid cylinder. EPR data of oligomers of various lengths labeled with this nitroxide showed size dependence supporting the hypothesis that the dynamics of the system arise from global tumbling. Local base motion was considered to be negligible in analyzing the double-stranded systems. However, dramatically increased motion was observed in the single-stranded spectrum. We have repeatedly observed this same effect of increased motion upon conversion of double-stranded DNA into single strands, and we attribute this to an increase in base motion.

The main criterion for which model applies to interpret EPR line shapes of spin-labeled nucleic acids seems to be a property of the tether. Base dynamics have been apparent with spin-labeled substrates that can be incorporated enzymatically and contain tethers of intermediate or low rigidity. These tethered nitroxides are positioned far enough away from the helix so as not to be significantly involved in any steric interactions and do not seem to perturb the DNA structure. On the other hand, a high-rigidity probe such as a nitroxide containing a two-atom acetylene tether is restricted by the sugar–phosphate backbone, which will result in a spectrum representing hindered local motion as well as global motion. Recently, Kirchner et al. (1990) published an EPR spectrum of a four-atom diacetylene-tethered nitroxide attached at position 5 of thymidylate that was incorporated into a dodecamer. The spectrum reveals increased motion over a similar system utilizing an acetylene tether. Spectral simulation gave a value of 5 ns for the isotropic correlation time representing cylinder diffusion, which is smaller than the range of values estimated previously for the acetylene-labeled dodecamer. We have simulated the published data according to our model and get a good simulation with a $\tau_{\perp}$ of about 4 ns. We believe that the enhanced motion is the result of the longer tether now allowing the nitroxide to monitor base dynamics.

The spin-labeling technique is a useful tool for elucidating structural and dynamic features of DNA. Spin labeling of bases with nitroxides containing tethers of low and intermediate rigidity permits the detection of base dynamics. When high rigidity tethers are used, base dynamics are no longer evident and global motion is predominantly monitored (Spaltenstein et al., 1989a). Our laboratory has focused attention on the more flexible nitroxides since analysis of the EPR line shapes can be used to obtain quantitative information about base motion. In the present study, nitroxide-labeled deoxycytidine analogues are incorporated enzymatically into $(dG\text{-}dC)_n$. Under appropriate salt conditions, the spin-labeled DNA can assume either B- or Z-conformations, which are readily verified by CD. EPR spectra of these two conformations are recorded and then analyzed with the base disk model. Spectral simulations indicate that local base motion in Z-DNA is about two times slower than in B-DNA.

Experimental Procedures

Materials. *Micrococcus luteus* DNA polymerase (EC 2.7.7.7) and [8-^{3}H]dGTP (specific activity 10 Ci/mmol) were purchased from ICN Biochemicals. *N*-Hydroxysuccinimide and *N*,*N*′-dicyclohexylcarbodiimide were obtained from Aldrich Chemical Co. $(dI\text{-}dC)_n$ and unlabeled nucleotides were purchased from Pharmacia LKB Biotechnologies. All other chemicals were purchased from either J. T. Baker Chemical Co., Fisher Scientific Co., Kodak Laboratory Chemicals, or Sigma Chemical Co. The synthesis of 2,5-dioxopyrrolidin-1-yl 2,2,6,6-tetramethyl-1-oxypiperidine-4-carboxylate (**1**), 5-(3-aminoprop-1-enyl)-2′-deoxycytidine 5′-triphosphate (**4**) and 5-[3-(2,2,6,6-tetramethyl-1-oxypiperidine-4-carboxamido)-prop-1-enyl]-2′-deoxycytidine 5′-triphosphate (**5**), and $(dG\text{-}dC,DCAT)_n$ has been described respectively by Toppin et al. (1986), Strobel et al. (1989), and Strobel et al. (1990).

2,5-Dioxopyrrolidin-1-yl 5-(2,2,6,6-Tetramethyl-1-oxypiperidine-4-carboxamido)pentanoate (**3**). By a procedural modification of Pauly et al. (1989), 117 mg (1.0 mmol) of 5-aminopentanoic acid in 4 mL of H_2O, saturated with triethylamine and adjusted to pH 10 with CO_2(g), was added to 150 mg (0.5 mmol) of **1** in 5 mL of *N*,*N*-dimethylformamide and stirred for 20 h at room temperature. Following solvent evaporation, the mixture was redissolved in 25 mL of H_2O (pH 9.0), adjusted to pH 10.3 with 1.0 M NaOH, and extracted with 2 × 25 mL of CH_2Cl_2. The aqueous layer was retained, acidified to pH 3 with 0.1 M HCl, and extracted with 4 × 25 mL of CH_2Cl_2. The clear orange organic layer was evaporated, resulting in 188 mg of 5-(2,2,6,6-tetramethyl-1-oxypiperidine-4-carboxamido)pentanoic acid (**2**) as a dark red oil. Without further purification, 175 mg (0.6 mmol) of **2**, 65 mg (0.6 mmol) of *N*-hydroxysuccinimide, and 124 mg (0.6 mmol) of *N*,*N*′-dicyclohexylcarbodiimide were dissolved in 7 mL of *N*,*N*-dimethylformamide and stirred for 22 h at 50 °C. Subsequent to 0 °C cooling for 15 min, the suspension was centrifuged, and 75 mg (0.19 mmol) of **3** was isolated as a red oil from the supernatant following preparative TLC (R_f 0.34): MS 396 (M^+). For a pictorial description of this procedure, see Scheme I.

5-{3-[5-(2,2,6,6-Tetramethyl-1-oxypiperidine-4-carboxamido)pentanamido]prop-1-enyl}-2′-deoxycytidine 5′-Triphosphate (**6**). The spin-labeled deoxycytidine analogue was formed by dissolving 4 mg (5.0 μmol) of **4** in 2 mL of 0.1 M sodium borate buffer (pH 8.7) and adding 10 mg (25 μmol) of **6** dissolved in 0.3 mL of *N*,*N*-dimethylformamide. The mixture was stirred at room temperature for 4 h, diluted with 15 mL of water, and purified by anion-exchange chromatography, yielding 1.0 mg (1.3 μmol) of **6**. Such quality was adequate for enzymatic incorporation; however, additional purification was required for NMR and kinetic analysis, and this was achieved either by reverse-phase HPLC or by ion-exchange FPLC: λ_{max} 284 nm in 0.04 M NH_4HCO_3 (pH 7.5); ^{1}H NMR 7.98 (C6), 1.29, 1.32, and 1.35 (12 nonequivalent piperidine CH_3 protons), 6.34 ppm (vinyl protons). The synthesis of **5** and **6** is diagrammatically presented in Scheme II.

Chromatographic Separations. Preparative TLC used to purify **3** was done on Analtech Uniplate 2000-μm silica gel GF (20 × 20 cm) plates and developed with MeOH–$CHCl_3$, 1:19 (v/v). Initial purification of **5** and **6** from the reaction mixture was achieved by loading the compounds onto Pharmacia DEAE-Sephadex A-25 (16 × 150 mm) ion-exchange resin and eluting with a 0.5-L linear gradient from 0.08 to 0.3 M NH_4HCO_3 (pH 7.5) at 1.6 mL/min. The same published procedure for with by reverse-phase HPLC (Strobel et al., 1989) was used for purifying **6**. A much less tedious method for purifying these spin-labeled nucleotides employed the Pharmacia FPLC Mono Q HR 5/5 (5 × 50 mm) anion-ex-

Scheme I: Synthesis of Activated Spin-Labeled Condensing Agent

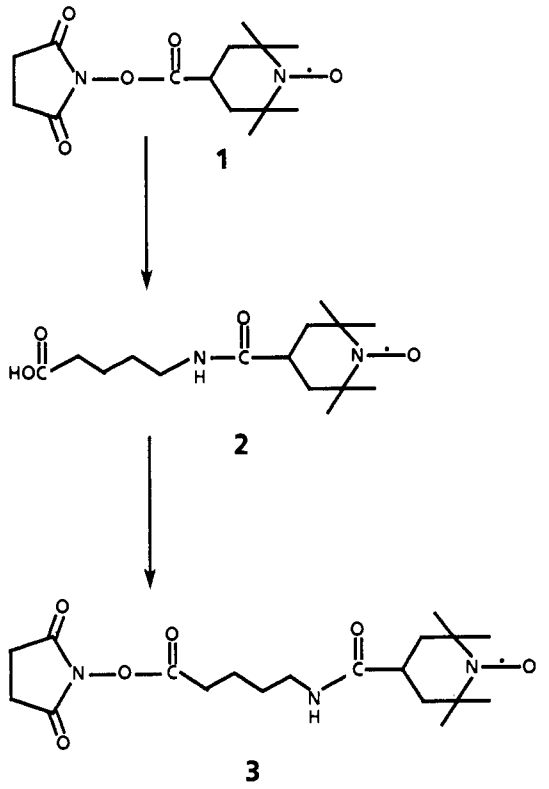

change resin. Up to 5 ODs at 1.0 OD/mL of **5** and **6** could successfully be loaded and resolved by employing the Pharmacia Super Loop. The products were eluted with gradients from 0.08 to 0.3 M NH_4HCO_3 (pH 7.5) at 1.0 mL/min and detected with a UV monitor set at 254 nm. A Pharmacia Sephacryl S-200 (16 × 360 cm) size exclusion column was used to separate the preparative scale (5×) polymerization products, $(dG\text{-}dC,dL)_n$ and $(dG\text{-}dC)_n$, from the unincorporated mononucleotides by eluting with 0.04 M NH_4HCO_3 (pH 7.5) at 0.5 mL/min.

Absorption and Circular Dichroism Spectra. UV absorption spectra were recorded on a Perkin-Elmer Lambda 5 UV–vis spectrophotometer. The concentrations for $(dG\text{-}dC,dL)_n$ and $(dG\text{-}dC)_n$ were calculated with $\epsilon = 8400\ M^{-1}\ cm^{-1}$ (Wells et al., 1970) and $\epsilon = 7300\ M^{-1}\ cm^{-1}$ (experimentally determined) at pH 7.0 for B- and Z-conformations, respectively. Digitized CD spectra were obtained with a Jasco J-500C spectropolarimeter interfaced with an IBM AT microcomputer, thereby facilitating baseline corrections and enhancing signal to noise through multiple scans. Polymers, at nucleotide concentrations of 50–150 μM, were scanned in a 1-cm path-length cell at room temperature.

NMR and Mass Spectrometry. Mass spectra were recorded on a Hewlett-Packard 5995 GC/MS via direct inlet sample introduction. NMR spectra were obtained by dissolving 0.1–0.2 mg of nucleotide triphosphate in 400 μL of D_2O and recording at 300 or 250 MHz with a Nicolet NTC-300 FT spectrometer or a Bruker AC-250 FT spectrometer, respectively. Chemical shifts are reported downfield from the internal standard, TMAC (3.20 ppm).

Experimental EPR Parameters. Spectra were obtained on a Bruker ESP 300 spectrometer outfitted with a Bruker TM_{110} cavity. The modulation amplitude and time constant were 1.6 G and 163 ms, respectively, and the microwave power was set below saturation of the samples at 30 mW.

Spectral Simulations. Spectral simulations were performed by using a simulation program developed by the Freed group (Polnaszek, 1976). Nitroxide EPR parameters were A_{xx} = 7.15 G, A_{yy} = 7.35 G, A_{zz} = 35.6 G, g_{xx} = 2.0088, g_{yy} = 2.0059, and g_{zz} = 2.0026. The input parameters were $\tau_{\parallel}$, $\tau_{\perp}$, tilt angle, and inhomogeneous broadening (T_2^{-1}). The line broadening (T_2^{-1}) was determined by fitting to the central line of the experimental spectra. The uncertainty in the τ values is on the order of 10%.

Preparation of Radiolabeled $(dG\text{-}dC)_n$ and $(dG\text{-}dC,dL)_n$.

Scheme II: Synthesis of Spin-Labeled dCTP Analogues

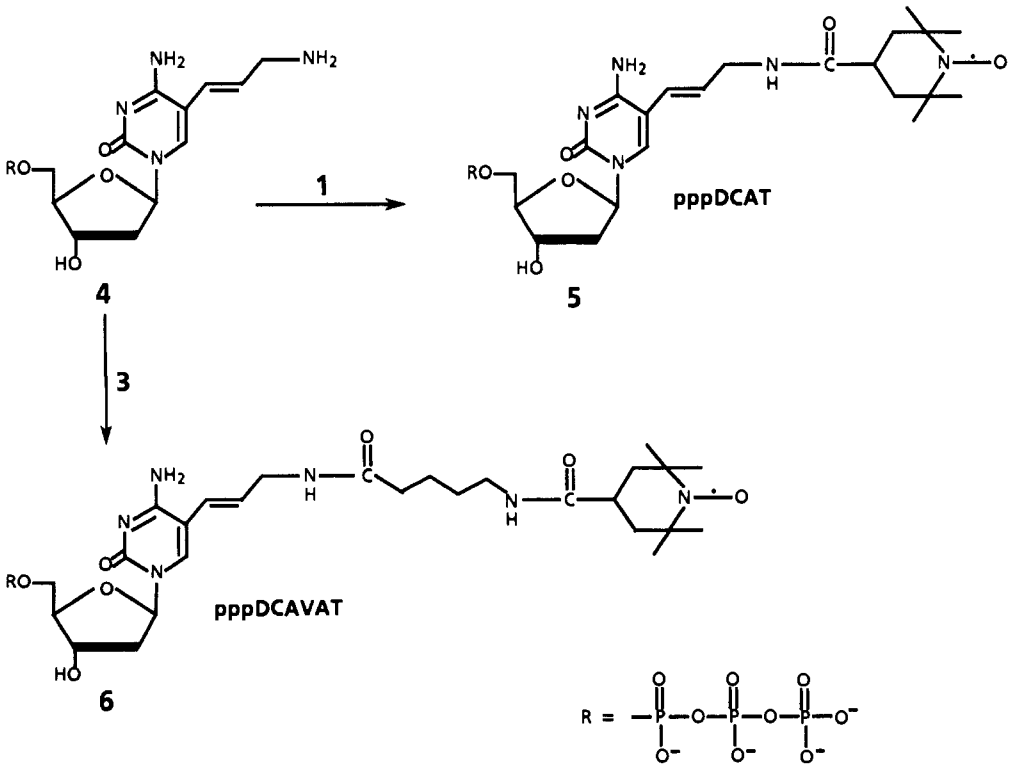

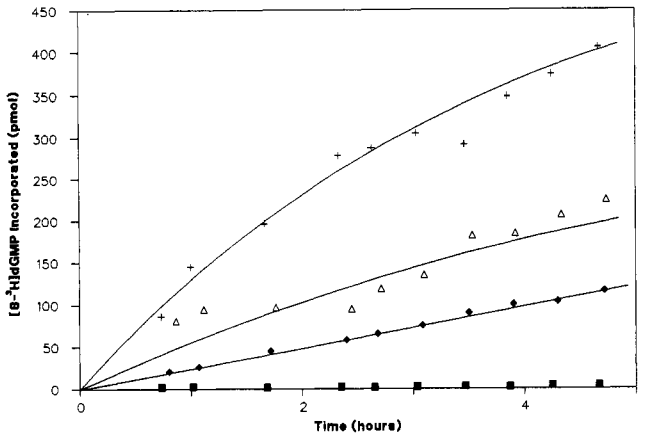

FIGURE 1: Polymerization dependence on type of spin label. Incorporation of [8-^{3}H]dGMP by *M. luteus* polymerase into (dG-dC,dL)$_n$ is plotted as a function of time. The deoxycytidine components of the reaction mixtures are as follows: (+) dCTP; (△) pppDCAVAT/dCTP, 5:1; (◆) pppDCAT/dCTP, 5:1; (■) no dCTP control.

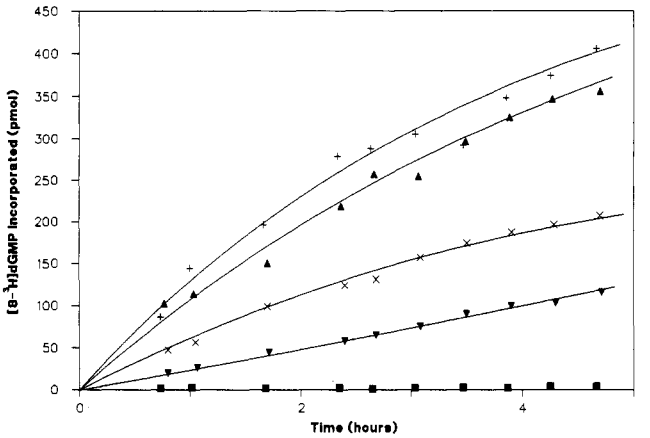

FIGURE 2: Polymerization dependence on spin-label concentration. Incorporation of [8-^{3}H]dGMP by *M. luteus* polymerase into (dG-dC,dL)$_n$ is plotted as a function of time. The deoxycytidine component compositions for the various reactions are given in nanomoles: (+) dCTP, 30; (▲) dCTP + pppDCAT, 30 + 50; (×) dCTP + pppDCAT, 30 + 75; (▼) dCTP + pppDCAT, 30 + 150; (■) no dCTP.

The scale of the radiolabeled polymerizations is one-fifth the scale used to produce preparative amounts of spin-labeled polymer. The 130-μL reactions were carried out in 1.5-mL polypropylene tubes and contained the following components (per reaction): 62 mM KH_2PO_4 (pH 7.5), 96 μM DTT, 5.8 mM $MgCl_2$, 60 nmol of [8-^{3}H]dGTP (specific activity 60 Ci/mol), 0–60 nmol of dCTP, 0–300 nmol of dLTP (HPLC or FPLC clean), 0.55 nmol of (dI-dC)$_n$ polymer, and 3 units of *M. luteus* DNA polymerase at 1 unit/μL buffered in 0.2 M KH_2PO_4 (pH 7.4), 0.1 M NaCl, 1.5 mM Na_2EDTA, and 50% (v/v) glycerin. The mixtures were incubated at 37 °C, and at appropriate time intervals, 3-μL samples were spotted on Whatman DE81 filters. The filters were successively washed in 2-mL aliquots with the following: 12 mL of 0.2 M Na_2HPO_4 (pH 7.5), 4 mL of H_2O, and 4 mL of 95% ethanol. After being dried under a heat lamp for 10 min, the filters were oven-dried at 50 °C for 4 h and counted in a toluene-based scintillation fluid (POPOP/PPO, 50 mg/L:4 g/L).

Preparation of Nonradiolabeled (dG-dC)$_n$ and (dG-dC,dL)$_n$. The original procedure, which utilizes (dI-dC)$_n$ as a template-primer for *M. luteus* polymerase for synthesizing (dG-dC)$_n$, was published by Wells et al. (1970). A modification of this protocol was used to prepare and isolate (dG-dC,-DCAT)$_n$, described by Strobel et al. (1990). This modified procedure was adapted to synthesize (dG-dC,DCAVAT)$_n$ and unlabeled (dG-dC)$_n$ by simply replacing equimolar amounts of pppDCAT with pppDCAVAT or dCTP to generate the respective alternating copolymers with approximately 0.5% label incorporation. *M. luteus* polymerase, purchased from Pharmacia (lot no. OM69820 and AC0698P01), was initially used in the polymerizations but was deemed unsuitable, since no high molecular weight polymers were synthesized as evidenced by size exclusion (Sephacryl S-200) liquid chromatography. The polymerase, obtained from ICN, catalyzed a 2-fold net synthesis of (dG-dC,dL)$_n$, which represents the use of 17% of the available triphosphates. Typical polymer lengths of approximately 20 000 base pairs were synthesized, and the sizes were calculated from final polymer concentrations and known starting amounts and lengths of primer-template.

Results

The small-scale (1×) radiolabeled polymerizations of this study were conducted primarily to determine the suitability of pppDCAT and pppDCAVAT as substrates for *M. luteus* polymerase and to optimize experimental conditions, with respect to label concentration and reaction time, for the large-scale (5×) polymerizations. Figure 1, a plot of [8-^{3}H]dGMP incorporation as a function of time, measures net polymer synthesis. At identical dCTP:dLTP molar ratios (5:1), both dCTP analogues support polymer production well above the baseline of a control reaction, which contains no deoxycytidine component. Also, from this plot it is obvious that pppDCAVAT is a better substrate than pppDCAT for this polymerase. In Figure 2, the effect of varying pppDCAT concentrations on polymer synthesis is illustrated by plotting [8-^{3}H]dGMP incorporation into (dG-dC,dL)$_n$ as a function of time. In each reaction mixture, except for the no dCTP control, the total amount of dCTP is a constant 30 nmol, and only the amount of pppDCAT is varied. As the pppDCAT quantity is increased from 0 to 300 nmol, the polymerization rate decreases. The polymerization kinetics at a pppDCAT/dCTP ratio of 2.5:1 is only slightly less than the observed kinetics where dCTP is the sole deoxycytidine-like component. The radiolabeling experiments helped optimize large-scale polymerization reaction times. The progress of polymer growth is normally determined by monitoring the reaction mixture for a hypochromic decrease in UV absorbance. Once the polymerase 3′–5′ exonuclease activity becomes dominant, loss of polymer is experienced and an increase in UV absorbance is observed. However, the presence of a strong UV-absorbing component in all mentioned polymerase preparations precluded the use of this method in the present study. Therefore, long-term radiolabeled experiments were conducted (data not shown) to determine the time and corresponding inflection point where exonuclease activity exceeded polymerase activity. Even after 36 h, no significant exonuclease activity was observed for any polymerizations utilizing spin-labeled substrates. Having established this, all preparative nonradiolabeled polymerizations were left to react, unmonitored, for up to 24 h.

The CD spectra of (dG-dC)$_n$, (dG-dC,DCAT)$_n$, and (dG-dC,DCAVAT)$_n$ in 0.1 M NaCl and 4.5 M NaCl are shown in Figure 3. The low salt spectra of all three polymers are typical of right-handed B-DNA, with positive peaks at 273 nm, negative peaks at 251 nm, and crossover points at 265 nm (±2 nm). When the polymers are subjected to high salt, the positive peak, negative peak, and crossover points of all three polymers move to 263, 292, and 278 nm (±2 nm), respectively. The observed near inversion of the CD spectra in response to an elevation of ionic strength indicates that each polymer is stabilized in the left-handed Z-conformation.

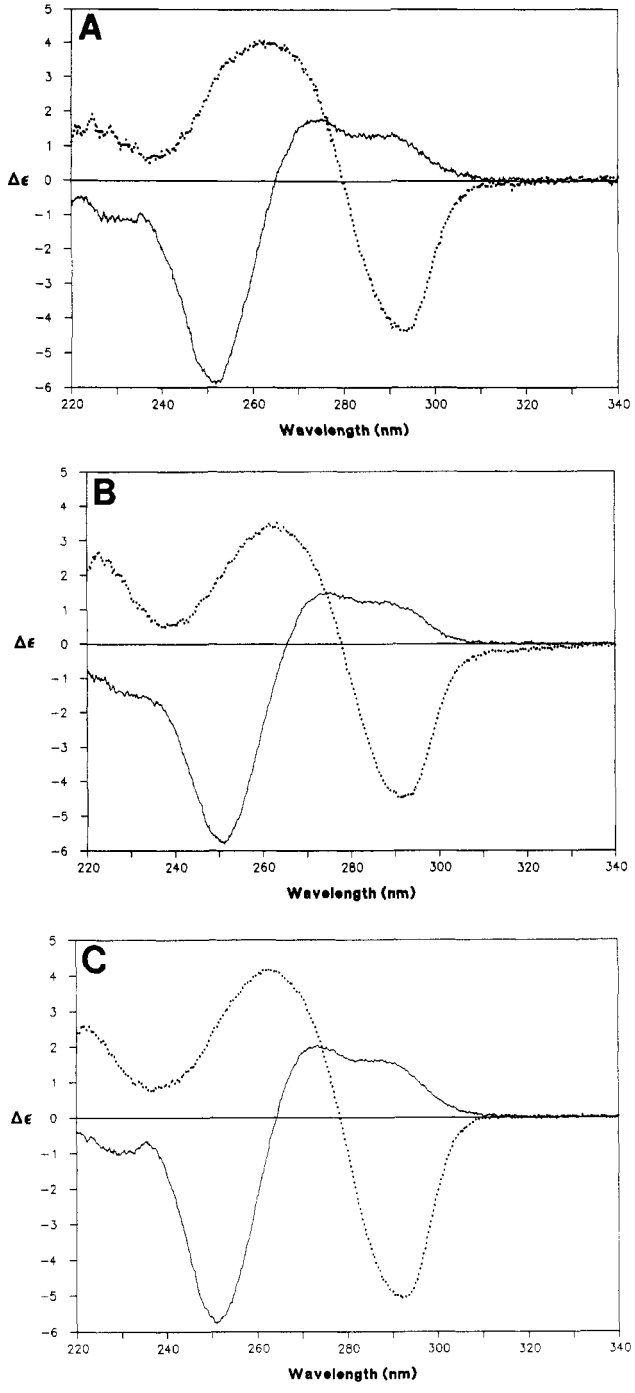

FIGURE 3: CD spectra of $(dG\text{-}dC,DCAT)_n$ (A), $(dG\text{-}dC,DCAVAT)_n$ (B), and $(dG\text{-}dC)_n$ (C) at room temperature as B-form in 0.1 M NaCl and 0.01 M sodium cacodylate, pH 7.0 (—), and as Z-form in 4.5 M NaCl and 0.01 M sodium cacodylate, pH 7.0 (···). The spectra are plotted as $\Delta\epsilon = \epsilon_L - \epsilon_R$ vs wavelength with baselines subtracted and concentrations normalized to 100 μM/base.

The EPR spectra of the two conformations of $(dG\text{-}dC,DCAT)_n$ are shown in Figure 4. The line shape of the Z-form represents slower motion as indicated by the decreased height ratios, h_+/h_0 and h_-/h_0, and line-shape broadening. This provides a unique EPR signature for Z-DNA labeled with DCAT. The experiment was repeated with the longer tethered DCAVAT. The spectra of $(dG\text{-}dC,DCAVAT)_n$ in low and high salt conditions are shown in Figure 5. It is clear that upon conversion from the B-form to the Z-form, the line shape undergoes a change qualitatively similar to that of $(dG\text{-}dC,DCAT)_n$. We have previously published the spectra of $(dA\text{-}dT,DUAT)_n$ under low and high salt conditions as a

FIGURE 4: Experimental (—) and computer-simulated (---) EPR spectra of 30 nmol of $(dG\text{-}dC,DCAT)_n$ at room temperature. The experimental spectra are recorded in either 4.5 M NaCl and 0.01 M sodium cacodylate, pH 7.0 (A), or 0.1 M NaCl and 0.01 M sodium cacodylate, pH 7.0 (B).

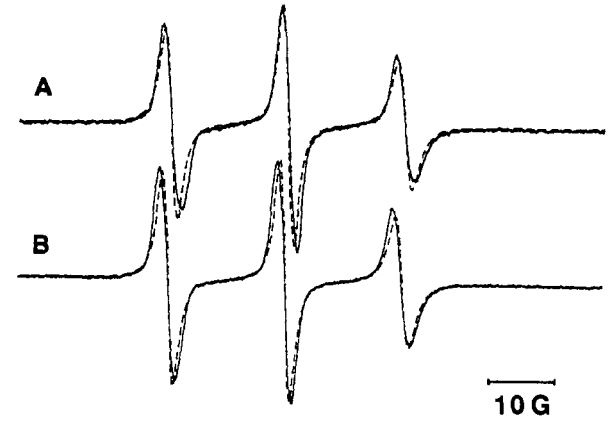

FIGURE 5: Experimental (—) and computer-simulated (---) EPR spectra of 30 nmol of $(dG\text{-}dC,DCAVAT)_n$ at room temperature. The experimental spectra are recorded in either 4.5 M NaCl and 0.01 M sodium cacodylate, pH 7.0 (A), or 0.1 M NaCl and 0.01 M sodium cacodylate, pH 7.0 (B).

control (Figure 2, Strobel et al., 1990). No significant change was observed in the line shape, indicating that the effect seen in Z-DNA is not a salt effect.

Interpretation of EPR spectra requires the implementation of an appropriate motional model to relate the line shape to nitroxide diffusion. This is accomplished by solving the equation of motion for the model describing this diffusion in terms of correlation functions. When an axially symmetric anisotropic model is used, the nitroxide diffusion is further correlated to the molecular diffusion of the labeled compound by a tilt angle. When the tilt angle is zero, then the nitroxide and molecular diffusion axes coincide. The correlation functions depend upon correlation times that indicate the rate of diffusion. In a Cartesian coordinate system, correlation times can be defined that describe diffusion around the principal axis, $\tau_\parallel$, and perpendicular to it, $\tau_\perp$ (Mason et al., 1974).

Simulated spectra are plotted along with the experimental spectra in Figures 4 and 5, and the motional parameters are tabulated in Table I. These results were interpreted according to the base disk motional model (see Figure 2, Kao et al., 1983). The data indicate that $\tau_\parallel$ is dependent on the spin-label tether; however, $\tau_\perp$ is independent of tether type and changes with changing conformation.

Discussion

The pioneering work of Kornberg and co-workers (Kelly et al., 1970) with DNA replication systems introduced the

Table I: Comparison of EPR Simulation Parameters and Experimental Data for B- and Z-DNA

compound	$\tau_{\parallel}$ (ns)	$\tau_{\perp}$ (ns)	tilt angle (±5°)	T_2^{-1}	h_+/h_0	h_-/h_0
B-DNA						
$(dG\text{-}dC,DCAT)_n$	0.2	4	50	0.8	0.92	0.26
$(dG\text{-}dC,DCAVAT)_n$	0.06	4	50	1	0.85	0.58
$(dA\text{-}dT,DUAT)_n$[a]	0.2	4	40	0.8	0.75	0.24
Z-DNA						
$(dG\text{-}dC,DCAT)_n$	0.2	7	40	0.8	0.55	0.18
$(dG\text{-}dC,DCAVAT)_n$	0.06	7	50	1	0.76	0.52

[a] Values previously reported by Pauly et al. (1987) and Kao and Bobst (1985). Simulation parameters and experimental data for $(dA\text{-}dT,DUAT)_n$ under high salt conditions are identical with those under low salt conditions.

possibility of incorporating radiolabeled nucleotides into DNA by enzymatic means. Since then, template/polymerase complexes have been utilized extensively to incorporate a wide variety of biotin-based nonradioactive nucleotides, to include affinity labels (Langer et al., 1981), photolabels (Forster et al., 1985), fluorescent labels (Hopman et al., 1986), chemiluminescent labels (Matthews et al., 1985), and electron-dense labels (Menissier et al., 1985). An excellent review of nonradioactive nucleic acid probes is provided by McInnes and Symons (1989).

Recently, Pauly et al. (1987) developed a series of 5-substituted thymidine triphosphate spin labels that were efficiently incorporated into synthetic and natural DNAs by a template-dependent prokaryotic polymerase. By similar methodology, the 5-substituted deoxycytidine triphosphates pppDCAT and pppDCAVAT were synthesized. As can be seen from Figure 1, these spin labels are also readily incorporated into DNA by *M. luteus* polymerase. Interestingly enough, the spin-labeled deoxycytidine and thymidine analogues share the same tether dependence on incorporation rate; namely, the longer tethered probes served as better substrates. It is possible that the longer tethered probes position the bulky nitroxide rings such that potential steric interferences are minimized between reporter molecule and replication complex.

Probe incorporation must be controlled such that the nucleic acid EPR-specific activity is high enough for detection and low enough to avoid spectral line broadening. From Figure 1, it is evident that the deoxycytidine spin probes, pppDCAT and pppDCAVAT, are readily incorporated by *M. luteus* polymerase, thereby imparting an EPR activity onto the synthetic DNAs that is well above that necessary for detection by modern EPR spectrometers. Under elevated (5:1) pppDCAT/dCTP concentrations, the polymerization continues at a somewhat reduced rate. But more importantly, the probability that incorporated spin labels reside in close proximity of one another on DNA, especially on an alternating copolymer, increases to such an extent that line-shape broadening may occur. This phenomenon has been previously observed for λ phage DNA labeled with DCAT and was attributed to Heisenberg spin exchange (Strobel et al., 1989). Therefore, in order to avoid spin exchange and label the DNA sufficiently for detection, a 1:1 mixture of pppDCAT and dCTP was used for the large-scale polymerizations. Polymerization kinetics for these experimental conditions can be extrapolated from Figure 2, which suggest that polymerase activity is similar when presented with either 100% dCTP or 1:1 pppDCAT/dCTP.

The CD spectra for the labeled and unlabeled polymers in Figure 3 are quite similar. All peak maxima, minima, and crossover point values are the same (±2 nm). Equally obvious are the inversions of the CD spectra for each polymer. The observed spectral inversion is a characteristic consequence of a B-Z transition and was first reported for $(dG\text{-}dC)_n$ by Pohl and Jovin (1972) and has since been used repeatedly as conformational verification of B- and Z-form DNA.

An important requirement of the spin-labeling technique is that the probe accurately report dynamics. Although the base disk model may at first sight appear simplified with only an effective tilt angle and two dynamic parameters ($\tau_{\parallel}$ and $\tau_{\perp}$), it essentially represents the limit to which a single EPR spectrum can be analyzed. This approach is corroborated by a study which showed how complex models of motional dynamics with many degrees of freedom can be reduced to just a few measurable parameters (Campbell et al., 1979). In the present case, we must ensure that the nitroxide is coupled to base motion and is not simply wobbling in the major groove. Currently, over 40 spin-labeled systems have been consistently analyzed with the base disk model. In all of these systems, $\tau_{\perp}$ has been found to be independent of tether length while $\tau_{\parallel}$ has shown tether dependence. The present data further confirm that the nitroxide monitors base motion. Specifically, as the DNA helix undergoes a transition from the right- to the left-handed form, the bases swing toward the surface of the helix, which places the nitroxide further from the helix. Molecular models showing this phenomenon have been published previously (Figure 3, Strobel et al., 1990). Thus, in the absence of coupling, $\tau_{\perp}$ would be expected to decrease as a result of less hindered motion of the probe. The raw data obtained with 5-atom and 11-atom tethered nitroxides clearly indicate the presence of a more hindered motion, which results in an increase in $\tau_{\perp}$ from 4 to 7 ns.

When B-DNA undergoes a transition to Z-DNA, there is a corresponding change in water structure. We do not believe that the motion difference is a result of this change since the effect is seen even when the 11-atom tethered DCAVAT is used as a spin label. Molecular modeling studies indicate that DCAVAT should place the nitroxide well beyond the hydration layers.

Local DNA dynamics have been interpreted as consisting of various internal modes. One set of these involves bending and torsional motions of the double helix (Barkley & Zimm, 1979). Barkley and Zimm described an elastic model which they showed to be formally equivalent to a bead-spring model. According to the spring model, the DNA helix is viewed as a series of base-pair oscillators coupled by springs with force constants that determine the dynamics. Another set of internal modes are the base pairs undergoing fluctuations. Examples of large fluctuations were observed by hydrogen-exchange experiments that have been modeled as two- and three-state opening and closing reactions of the individual bases (Englander & Kallenbach, 1984; Hartmann et al., 1986). This type of motion seems to be consistent with viewing the base pair as two separate base oscillators. In this scheme, each strand behaves as a separate series of oscillators with the sugar–phosphate backbone acting as the axis. In view of light scattering results which indicate an increase in persistence length upon conversion from the B-form to the Z-form (Thomas & Bloomfield, 1983), the Barkley–Zimm model would predict that an increase in the spring constants would account for the increase in rigidity. This would result in an increase in frequency of bending and torsions. While the Barkley–Zimm model describes the dynamics of the double helix, individual base dynamics may be independent of helical torsions and bending. Therefore, the slower base motions that we have observed in Z-DNA may not be directly related to

the increase in helix rigidity. This interpretation is in qualitative agreement with hydrogen-exchange experiments where exchange was slower for Z-DNA than for B-DNA (Ramstein & Leng, 1980; Ramstein et al., 1985) although the time scale for hydrogen exchange is slower than for EPR.

In conclusion, the EPR spectra of $(dG\text{-}dC,DCAT)_n$ and $(dG\text{-}dC,DCAVAT)_n$ can provide unique signatures for detecting Z-DNA as corroborated by CD analysis. The EPR line shapes indicate that the nitroxide motion in Z-DNA is slower than in B-DNA. According to the base disk motional model, the base dynamics are about two times slower in Z-DNA.

ACKNOWLEDGMENTS

We thank Dr. Dave Behnke of the University of Cincinnati College of Medicine for providing assistance with preliminary CD data. We also thank the Procter and Gamble Co. of Cincinnati, OH, for use of their CD polarimeter and Dr. Curt Marcott for his technical assistance.

REFERENCES

Barkley, M. D., & Zimm, B. H. (1979) *J. Chem. Phys. 70*, 2991–3007.

Bobst, A. M., Pauly, G. T., Keyes, R. S., & Bobst, E. V. (1988) *FEBS Lett. 228*, 33–36.

Campbell, R. F., Meirovitch, E., & Freed, J. H. (1979) *J. Phys. Chem. 83*, 525–533.

Drew, H., Takano, T., Tanaka, S., Itakura, K., & Dickerson, R. E. (1980) *Nature 286*, 567–573.

Englander, S. W., & Kallenbach, N. R. (1984) *Q. Rev. Biophys. 16*, 521–655.

Forster, A. C., McInnes, J. L., Skingle, D. C., & Symons, R. H. (1985) *Nucleic Acids Res. 13*, 745–761.

Hall, K., Cruz, P., Tinoco, I., Jr., Jovin, T. M., & van de Sande, J. H. (1984) *Nature 311*, 584–586.

Hartmann, B., Leng, M., & Ramstein, J. (1986) *Biochemistry 25*, 3073–3077.

Hopman, A. H. N., Wiegant, J., Tesser, G. I., & Van Duijn, P. (1986) *Nucleic Acids Res. 14*, 6471–6488.

Ikuta, S., & Wang, Y.-S. (1989) *Nucleic Acids Res. 17*, 4131–4144.

Kao, S.-C., & Bobst, A. M. (1985) *Biochemistry 24*, 5465–5469.

Kao, S.-C., Polnaszek, C. F., Toppin, C. R., & Bobst, A. M. (1983) *Biochemistry 22*, 5563–5568.

Kelly, R. B., Cozzarelli, N. R., Deutscher, M. P., Lehman, I. R., & Kornberg, A. (1970) *J. Biol. Chem. 245*, 39–45.

Kirchner, J. J., Hustedt, E. J., Robinson, B. H., & Hopkins, P. B. (1990) *Tetrahedron Lett. 31*, 593–596.

Kochel, T. J., & Sinden, R. R. (1989) *J. Mol. Biol. 205*, 91–102.

Langer, P. R., Waldrop, A. A., & Ward, D. C. (1981) *Proc. Natl. Acad. Sci. U.S.A. 78*, 6633–6637.

Marx, J. L. (1985) *Science 230*, 794–796.

Mason, R. P., Polnaszek, C. F., & Freed, J. H. (1974) *J. Phys. Chem. 78*, 1324–1329.

Matthews, J. A., Batki, A., Hynds, C., & Kricka, L. J. (1985) *Anal. Biochem. 151*, 205–209.

McInnes, J. L., & Symons, R. H. (1989) in *Nucleic Acid Probes* (Symons, R. H., Ed.) pp 33–80, CRC Press, Inc., Boca Raton, FL.

Menissier, J., Hunting, D. J., & De Murcia, G. (1985) *Anal. Biochem. 148*, 339–343.

Mirau, P. A., Behling, R. W., & Kearns, D. R. (1985) *Biochemistry 24*, 6200–6211.

Pauly, G. T., Thomas, I. E., & Bobst, A. M. (1987) *Biochemistry 26*, 7304–7310.

Pauly, G. T., Bobst, E. V., Bruckman, D., & Bobst, A. M. (1989) *Helv. Chim. Acta 72*, 110–116.

Pohl, F. M., & Jovin, T. M. (1972) *J. Mol. Biol. 67*, 375–396.

Polnaszek, C. F. (1976) Ph.D. Thesis, Cornell University, Ithaca, NY.

Ramstein, J., & Leng, M. (1980) *Nature 288*, 413–414.

Ramstein, J., Vogt, N., & Leng, M. (1985) *Biochemistry 24*, 3603–3609.

Spaltenstein, A., Robinson, B. H., & Hopkins, P. B. (1989a) *Biochemistry 28*, 9484–9495.

Spaltenstein, A., Robinson, B. H., & Hopkins, P. B. (1989b) *J. Am. Chem. Soc. 111*, 2303–2305.

Strobel, O. K., Bobst, E. V., & Bobst, A. M. (1989) *Arch. Biochem. Biophys. 273*, 597–601.

Strobel, O. K., Keyes, R. S., & Bobst, A. M. (1990) *Biochem. Biophys. Res. Commun. 166*, 1435–1440.

Thomas, T. J., & Bloomfield, V. A. (1983) *Nucleic Acids Res. 11*, 1919–1930.

Toppin, C. R., Pauly, G. T., Devanesan, P., Kryak, D., & Bobst, A. M. (1986) *Helv. Chim. Acta 69*, 345–349.

Wahl, Ph., Paoletti, J., & Le Pecq, J.-B. (1970) *Proc. Natl. Acad. Sci. U.S.A. 65*, 417–421.

Wang, A. H.-J., Quigley, G. J., Kolpak, F. J., Crawford, J. L., van Boom, J. H., van der Marel, G., & Rich, A. (1979) *Nature 282*, 680–686.

Wells, R. D., Larson, J. E., Grant, R. C., Shortle, B. E., & Cantor, C. R. (1970) *J. Mol. Biol. 54*, 465–497.

Zacharias, W., Jaworski, A., Larson, J. E., & Wells, R. D. (1988) *Proc. Natl. Acad. Sci. U.S.A. 85*, 7069–7073.